ROTORBLADE SHAPE ESTIMATION WITH FIBER-OPTICAL SENSORS FOR A HEALTH AND USAGE MONITORING SYSTEM

Soeren Suesse
soeren.suesse@tum.de
Research Assistant

Manfred Hajek
hajek@tum.de
Full Professor

Institute of Helicopter Technology
Technical University of Munich
Germany

Abstract

The increasing maturity and decreasing size of the measurement equipment enables Fiber Bragg Grating (FBG) sensors to be used for structural monitoring of complex structures. FBGs applied on helicopter rotor blades are used to identify blade movements, which will serve as a valuable data source to supply Usage Monitoring Systems for rotorcraft. In this paper, a modified approach is presented that calculates the displacement of a rotor blade with nonuniform cross sections in two dimensions, based on surface strain measurements with FBGs. Furthermore, the effect of different boundary conditions and sensor combinations is analyzed.

NOTATION

CFRP	Carbon-Fiber–Reinforced Polymer
c_i	Distance between neutral fiber and sensor at cross section i, m
D	Normalised strain, $(m/m)/m$
ϵ_i	Measured strain at cross section i, (m/m)
Δl	Distance between adjacent sensors along the wing-span, m
S_{a_i}	Measured strain at sensor i for load case a, (m/m)
y_i	Displacement at cross section i, m
y_{a_i}	Distance between neutral fiber and sensor i, m
Θ_i	Slope at cross section i, deg

1 INTRODUCTION

Monitoring the deflection of arbitrary-shaped aircraft structures in real-time allows to improve performance and safety of these structures and might even be used for usage monitoring to extend life time credit for parts of the aircraft. The break-up of the NASA Helios Prototype in 2003 is one example of an application, where the use of real-time structural health monitoring might have avoided the accident [1].

In the last years, the development of Health and Usage Monitoring Systems (HUMS) for rotorcraft was focused primarily on monitoring gearboxes and drive trains. For example, an amendment proposed by EASA for CS-29 in 2010 covered mainly vibration health monitoring of the drive train [2]. With the use of new technologies like fiber-optical sensors, integrated into and applied to rotor blades [3], it might be possible to realize a direct measurement of loads for the use in a Health and Usage Monitoring System. Using fiber-optical sensors for deflection measurements offers advantages over other technologies. Cameras for deflection monitoring might be installed for flight tests, but are impractical for permanent installation [4]. Fiber-optical sensors also have a weight benefit over conventional strain gauges since less wiring effort is needed for the same amount of sensors. It is possible to integrate multiple sensors into one fiber over a length of several meters.

Previous research describes the use of displacement-strain transformations for calculating displacements based on measured strains in fiber-optical sensors. Two individual approaches are primarily used for strain-displacement calculation. The Ko Displacement Theory [5], also referenced as "FOSS Algorithm", with additional changes in other publications, uses closed-form equations to calculate displacements using surface strain data. The second method takes displacement and strain matrices of mode shapes to estimate

the displacement at given points [6, 7]. While the research up to the present was conducted mainly on cantilever beams with uniform cross sections, made of a single material, this paper demonstrates the application on a rotor blade made of composite materials and with nonuniform cross sections. Furthermore, the rotor blade is tapered and twisted. The approach is extended in this paper to account for displacement in two dimensions, which is of importance for rotor blades; in contrast to fixed wing displacement which occurs mainly in one direction. Strain-Displacement transformations based on measurements on the rotor blade might be used to estimate loads in real-time, which in turn would be an important step forward towards usage monitoring of the rotor system and the rotorcraft. Another possible application of the method presented in this paper could be the estimation of the rotor tip clearance of coaxial rotorcrafts [8].

2 MATHEMATICAL BACKGROUND - EXTENDING THE KO DISPLACEMENT THEORY

In this chapter, the mathematical part of the original Ko Displacement theory [5] is extended to calculate the position of the neutral axis, strain field and displacement of the structure in two dimensions.

2.1 Overview Method

In the following, the process to get from a strain measurement at discrete points on the surface of a structure to the calculated deflection of the structure in two dimensions is presented. An overview of the method is shown in a flowchart in Fig. 1. The first step is determining the location of the neutral axis by measuring the strain at each sensor position for two load cases, which must be linearly independent. By solving an equation system with ten equations, the location of the neutral axis can be determined in two directions at each cross section if at least three sensors are available per cross section. It is possible to apply voting or "best fit" algorithms in this step to detect erroneous sensors or refine the solution by using different sensor combinations.

The location of the neutral axis and the strain measurements of all sensors of one cross section are used to calculate a two-dimensional strain field for each cross section with sensors. This strain field will be used afterwards to calculate the displacement of each section and by integrating over the length, the displacement of the whole beam/rotor blade. If more than two sensors per cross section are installed, different sensor combinations can be utilized to detect erroneous sensor signals and potentially improve the results.

For this paper, the calculated displacement was compared to the results of photogrammetry measurements. The error was compared separately for both directions, Y and Z.

2.2 Determining the Location of the Neutral Axis

In order to be able to calculate the displacement in each direction, the distance from each sensor to the neutral axis has to be known. Most other applications of the Ko-Displacement Theory are based on rectangular cross sections or displacement observations in only one direction, where it is possible to determine the position of the neutral axis with one load case and two sensors. In this case, the cross sections are airfoil-shaped (see Fig. 2) and are varying over the length of the rotor blade in span-wise direction.

Therefore, the location of the neutral axis changes along the wingspan and has to be determined for each cross section in Y- and Z- direction. The following equation system was developed for this purpose. Two linearly independent strain measurements (S_1 and S_2) have to be conducted to receive ten linear independent equations to solve for the unknown distance y_{a_i} and z_{a_i} from each sensor i to the neutral axis in Y- and Z-direction

$$S_{1_i} = D_{1_y} \cdot y_{a_i} + D_{1_z} \cdot z_{a_i} \tag{1}$$

$$S_{2_i} = D_{2_y} \cdot y_{a_i} + D_{2_z} \cdot z_{a_i} \tag{2}$$

for n sensors $i = 1, 2, 3, 4, .., n$. D is the normalized strain in y-direction, respectively z-direction and is also an unknown variable. Together with the relation between the known global coordinates of the sensor positions, respectively the distance between two sensors

$$y_{a_1 a_2} = |y_{a_1} - y_{a_2}| \tag{3}$$

$$y_{a_1 a_3} = |y_{a_1} - y_{a_3}| \tag{4}$$

$$z_{a_1 a_2} = |z_{a_1} - z_{a_2}| \tag{5}$$

$$z_{a_1 a_3} = |z_{a_1} - z_{a_3}| \tag{6}$$

is known and the equation system can be solved. For this paper, the minimum amount of $n = 3$ sensors has been used to determine the exact solution of the equation system with ten equations and ten unknown variables. The results of the calculation are discussed later in Section 4.2.

Theoretically, the calculation has to be done only once, for example on ground. Therefore, this calculation is not critical for any real-time operation of a future Health and Usage Monitoring System. The availability of three sensors is necessary; four or more sensors per cross section would be even better since it was possible to compare the results and identify faulty sensors.

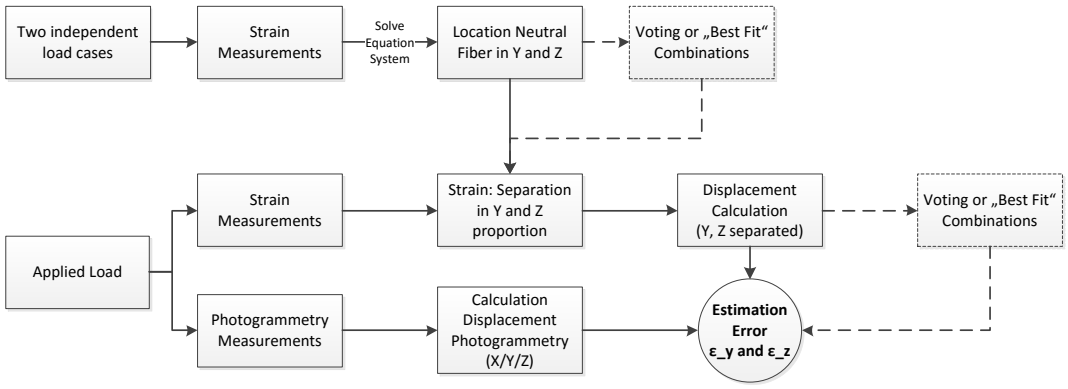

Figure 1: Flowchart of the method to solve for displacement in two directions.

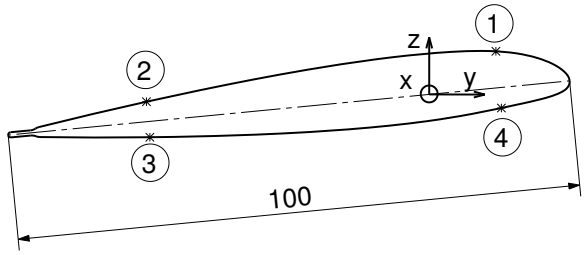

Figure 2: Cut through the rotor blade at $x = 300$ mm with typical sensor distribution.

2.3 Dividing Bending in Y- and Z-Direction

The Ko Displacement Theory has been mainly used to calculate the displacement in one direction. In this paper, the displacement is calculated in two directions, Y and Z. The strain value, measured at FBG sensor, has to be split into a proportion in Y- and Z-direction:

$$S_{a_1} = D_y \cdot y_{a_1} + D_z \cdot z_{a_1} \tag{7}$$

$$S_{a_2} = D_y \cdot y_{a_2} + D_z \cdot z_{a_2} \tag{8}$$

$$S_{a_i} = D_y \cdot y_{a_i} + D_z \cdot z_{a_i} \tag{9}$$

S_{a_i} is the measured strain value in $[m/m]$ at sensor i and y_{a_i} respectively z_{a_i} the distance between the sensor i and the location of the neutral axis at this cross section. The set of equations is solved for D_y and D_z which are normalized values of the strain $[(m/m)/m]$, independent of the distance from the neutral axis in Y and Z direction.
To solve the set of equations, a minimum of two sensors is required. With a multivariate linear regression, the equation system can also be solved with more than two sensors. The quality of the results might be improved and smoothed by using more than the minimum of two sensors. In this paper, results are shown for $n = 2, 3, 4$ sensors per cross section.

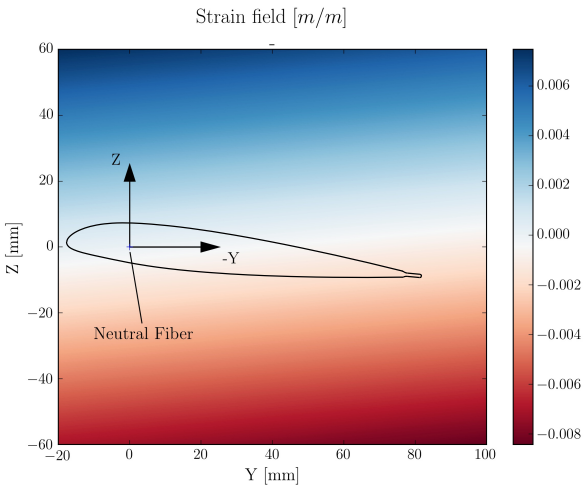

Figure 3: Exemplary two-dimensional linear strain field in Y- and Z-direction. In this example, a point load in Z-direction was applied to the free end of the blade.

An exemplary resulting strain field is shown in Fig. 3. For this figure, the strain value S_{a_i} of equation 9 was determined for each point in Y- and Z-direction with the calculated values of D_y and D_z. It can be seen that the gradients of the strain field are increasing mainly in Z-direction, though there is also a slight gradient in Y-direction (the corresponding displacement curve can be seen in Fig. 10). This is due to the fact that the load applied was a single load in Z-direction, applied to the wing tip of the rotor blade. The benefit of using a normalized two-dimensional strain field is being independent in placing the sensors at any discretionary position on the surface or into the structure. Additionally, using normalized values for the strain field makes it possible to compare the results of different sensor combinations, even if the sensors are located on arbitrary points at each cross section.

2.4 Calculating the Displacement in each Direction

The approach to estimate the deflection of fixed wings by measuring strain at discrete points on the surface, is known as the Ko Displacement Theory. The theory is derived from the Euler-Bernoulli beam theory and discretizes the beam differential equation.

$$\frac{\mathrm{d}^2 y}{\mathrm{d}\, x^2} = \frac{M(x)}{EI} \tag{10}$$

Ko and Fleischer developed this equation further for nonuniform cantilever beams [9]. The displacement y is calculated with the slope $\tan\Theta_i$, the measured strain ϵ_i, the distance from the neutral axis c_i at position i and the length Δl_i between cross section i and $i-1$:

$$y(x) = \int_{x_{i-1}}^{x_i} \tan\Theta(x)\, \mathrm{d}\, x + y_{i-1} \tag{11}$$

with the slope equation

$$\begin{aligned}\tan\Theta(x) &= \int_{x_{i-1}}^{x_i} \frac{\epsilon(x)}{c(x)} dx + \tan\Theta_{i-1} \\ &= \Delta l_i \left[\frac{\epsilon_{i-1}-\epsilon_i}{c_{i-1}-c_i} + \frac{\epsilon_{i-1}c_i - \epsilon_i c_{i-1}}{(c_{i-1}-c_i)^2} log_e \frac{c_i}{c_{i-1}}\right] \\ &\quad + \tan\Theta_{i-1}\end{aligned} \tag{12}$$

For slightly non-uniform cantilever beams where the cross-sections change slowly [10], the equations can be simplified to

$$\begin{aligned}\tan\Theta_i &= \frac{\Delta l_i}{2c_{i-1}} \left[\left(2 - \frac{c_i}{c_{i-1}}\right)\epsilon_{i-1} + \epsilon_i\right] \\ &\quad + \tan\Theta_{i-1}\end{aligned} \tag{13}$$

$$\begin{aligned}y_i &= \frac{(\Delta l_i)^2}{6c_{i-1}} \left[\left(3 - \frac{c_i}{c_{i-1}}\right)\epsilon_{i-1} + \epsilon_i\right] \\ &\quad + y_{i-1} + (\Delta l_i)\tan\Theta_{i-1}\end{aligned} \tag{14}$$

By using the approach of a normalized strain field D (see Section 2.3), c can be set to an arbitrary value $c = constant$ and ϵ is substituted by the normalized strain value D_y, respectively D_z:

$$\tan\Theta_i = \frac{\Delta l_i}{2c_{i-1}} \left(D_{y_{i-1}} + D_{y_i}\right) + \tan\Theta_{i-1} \tag{15}$$

$$\begin{aligned}y_i &= \frac{(\Delta l_i)^2}{6c_{i-1}} \left(2 \cdot D_{y_{i-1}} + D_{y_i}\right) \\ &\quad + y_{i-1} + (\Delta l)\tan\Theta_{i-1}\end{aligned} \tag{16}$$

2.5 Possible Sensor Combinations

An advantage of the method presented is the ability to compare the results at each step among different sensor combinations. Particularly with critical systems (like a Health and Usage Monitoring System which might provide lifetime credit in the future), it is important to have redundant data. Firstly, to be able to detect faulty sensors and data, by means of a voting algorithm and secondly, to be able to still perform displacement calculations even if one or more sensors are not available anymore. Below, the number of possible independent sensor combinations is determined for different situations and cases.

2.5.1 Neutral Axis

The calculation of the position of the neutral axis in Y- and Z-direction requires a minimum of three sensors per cross section. The number of possible combinations is

$$\frac{n!}{(n-m)!\cdot m!} \tag{17}$$

with n total sensors per cross section and m sensors used for each calculation. For this paper, $m = 3$ sensors were used for the calculation of the neutral axis. Thus, there are four possible combinations. The number of possible combinations for different numbers of sensors per cross section is shown in Table 1. In order to be able to compare results from the computation of the neutral axis, at least four sensors per cross section are required.

Number of sensors n	Combinations for $m = 3$	Combinations for $m = 3, ..., n$
3	1	1
4	4	5
5	10	16
6	20	42
7	35	99

Table 1: Number of possible combinations to calculate the position of the neutral axis. m is the number of sensors per cross section which is used for the calculation.

In order to get more possible combinations, it would be possible to use, for example, a multivariate linear regression to solve the equation system in Section 2.2. In this case, the number of possible combinations would be

(18) $$\sum_{m=3}^{m=b} \frac{n!}{(n-m)! \cdot m!}$$

with n being the number of sensors per cross section, b the maximum number of sensors which shall be used for the multivariate regression (normally $b = n$) and m the number of sensors used for each calculation. The resulting possible combinations for this case are displayed in the last column of Table 1.

2.5.2 Strain Field

For the calculation of the strain field and hence, the displacement, a minimum of two sensors per cross section is needed. The number of possible combinations for a cross section with n sensors is

(19) $$\sum_{m=a}^{m=b} \frac{n!}{(n-m)! \cdot m!}$$

where m is the number of sensors used for the strain field calculation, a the minimum number of sensors used for the calculation and b the maximum number of sensors which shall be used for the calculation. For this paper, values of $a = 2$ and $b = 4$ were used. With a total number of $n = 4$ sensors, the amount of possible combinations is 11.

Possible combinations for $b = n$ sensors:

Number of sensors n	$a = 2$	$a = 3$	$a = 4$
2	1	-	-
3	4	1	-
4	11	5	1
5	26	16	6
6	57	42	22

Table 2: Number of possible combinations to calculate displacement in two directions for $b = n$ sensors per cross section.

Later, it will be shown, that a minimum of $a = 3$ sensors is needed to minimize the displacement error. Which means, on the other hand, that at least four sensors per cross section are needed to be able to compare the results of the displacement calculations. Such a comparison could be useful for a voting algorithm or to improve the quality of the results.

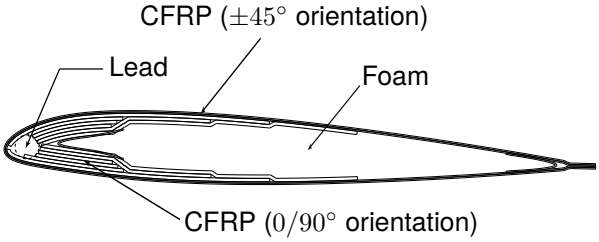

Figure 4: Cut through the homogeneous section of the rotor blade at $x = 1000$ mm [11].

3 EXPERIMENTAL SETUP

3.1 Rotor Blade

The rotor blade used for the tests was developed at the Technical University of Munich for the Flettner rotor of a civil drone with a mass of 30 kg. The rotor blade has a length of 1550 mm and consists of a complex buildup of carbon fiber layers, a rigid foam core and lead at the leading edge at the outer radial section. A cut through the homogeneous part of the rotor blade is shown in Fig. 4. The skin and innermost layers are made of $\pm 45°$ CFRP layers, while the mid layers are of $0/90°$ orientation. The rotor blade has a twist of $10°$ and taper beginning at 60% of the rotor blade length. As a side note: The plots in the results section start at $x = 136$ mm and not at $x = 0$ mm due to the fact that here, the z-axis is defined as the vertical rotor axis of the rotor system.

3.2 Photogrammetry

For the photogrammetry, a system from AICON 3D Systems was used. The photogrammetry targets (see Fig. 5) were applied to the upper and lower surface of the rotor blade and the stationary surroundings. The distribution of the targets was similar to the one of the sensors. For each load step, 80-120 photogrammetry images were taken. With this amount of pictures taken, the accuracy of the photogrammetry measurements could be improved. The error of this system for the experimental tests in this paper is negligible (one standard deviation of approximately $0.015 - 0.020$ mm) compared to the other measurement errors.

3.3 FBG Sensors

3.3.1 Equipment

The measurement device used for the tests was a "FBGS FBG-scan 804D", operating at a wavelength range between 1510 and 1590 nm. The spectrometer has four parallel inputs for optical fibers with a maximum scan rate of 500 Hz and 40 sensors per fiber.

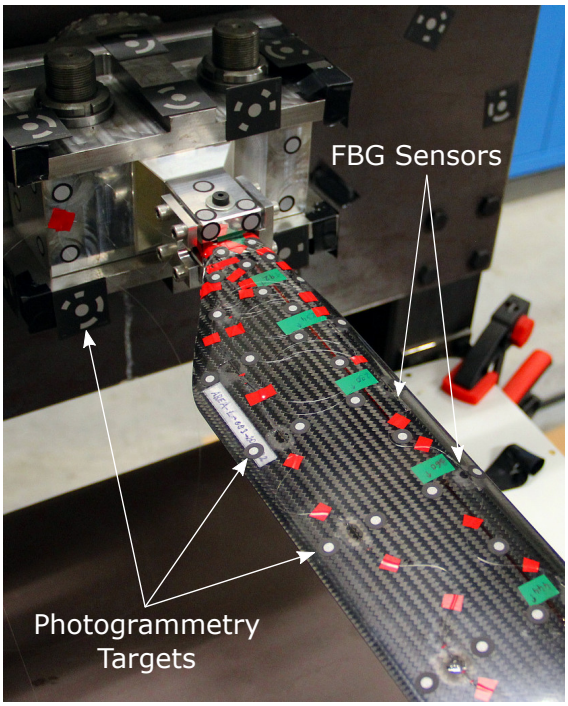

Figure 5: Rotor blade test bench with optical fibers and bonded photogrammetry targets. Two optcal fibers were applied to the upper surface and two to the bottom surface.

3.3.2 Sensor Distribution

For the strain-displacement tests, four optical fibers were applied span-wise to the wing surface. The direction of all sensors was oriented parallel to the x-axis. Two sensors were placed near the leading edge at the top and bottom surface, the other two sensors are located near the trailing edge, also on the top and bottom. The sensor positions are shown in Fig. 6. Along the wing-span, sensors were positioned at 15 cross-sections. For this paper, the sensors at the last cross section near the blade tip were not bonded to the surface, so they were only used to measure the impact of temperature on the overall measurements. The distances between the sensors vary along the wing-span: One third of the sensors are positioned at the inhomogeneous section close to the blade root, where the curvature of the blade and the strain gradients are expected to be the highest. The rest of the sensors are distributed with increasing spacing towards the blade tip. Theoretically, less sensors would be required along the radius, especially if only a static, single force is applied at the end of the rotor blade. For this paper, more sensors were already applied to the rotor blade since dynamics and higher-harmonics are going to be examined in upcoming studies.

4 RESULTS AND DISCUSSIONS

The results of the whole chain from calculating the neutral axis to the displacement are presented in this chapter. Furthermore, studies regarding the sensitivity of certain changes to the boundary conditions and sensor combinations are shown.

4.1 Test Cases

The test campaign for this research of the displacement in two directions comprises of 36 different load cases. In all cases, a single force was applied to the tip of the rotor blade. Three main factors were varied: Firstly the force, ranging from 10 N to 80 N; secondly, small variations of the angle of attack of the force to regard for different effects on the blade twist due to the blade's tapered and twisted geometry and thirdly, the main direction of the force (Z or Y). In flight, the main force will be exerted in Z direction, though, test were conducted also with main forces in Y-direction. In this paper, one of the load cases is shown with a main force in Z-direction; however, the conclusions presented are valid for all test cases which were examined.

4.2 Neutral Axis Calculation

The neutral axis was determined using two independent load cases and all four possible combinations with three sensors per combination. Furthermore, the average of all four combinations was calculated. The results for each of the 14 cross sections and five combinations are shown in Fig. 7. The values are the distances from the x-axis in Z-, respectively Y-direction. For both directions, Z and Y, the location of the neutral axis varies over the radius of the rotor blade. This was expected due to changes in the geometry and the materials over the wing-span. There are differences visible between the sensor combinations: Both combinations with two sensors at the trailing edge and one sensor at the leading edge (sensor combinations 1/2/3 and 2/3/4) show the highest deviations in most cases. Interestingly, the absolute value of the deviations from the average is almost identical in all cases for these two combinations. A reason for these deviations could be that the strain field is not as linear as assumed. This behavior appears mostly for sensor combinations which involve two outer sensors near the trailing edge. Another explanation for this behavior are measurement errors when the sensors were bonded to the surface and the coordinates of the sensors in Y-direction were measured manually by hand. Below, the displacement calculations are performed with all five combinations to examine the effect of the neutral axis location on the displacement error for each combination.

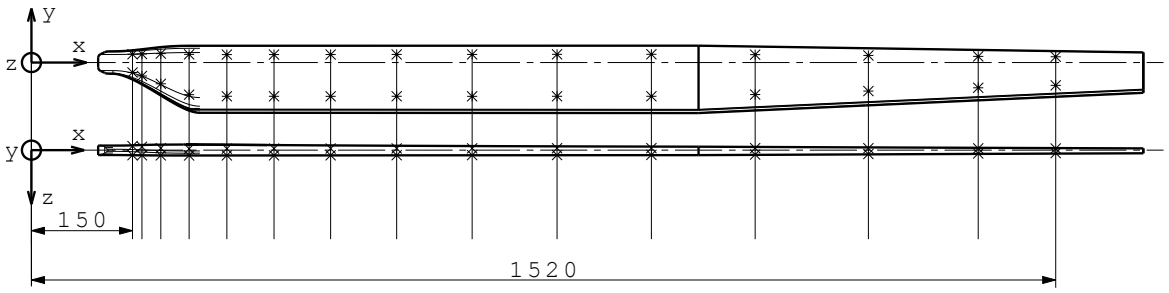

Figure 6: Sensor distribution along the wingspan. The Z-axis coincides with the rotor axis. Therefore, the rotor blade does not begin at 0 mm. Two optical fibers were applied to the upper surface and two to the bottom surface at each cross section.

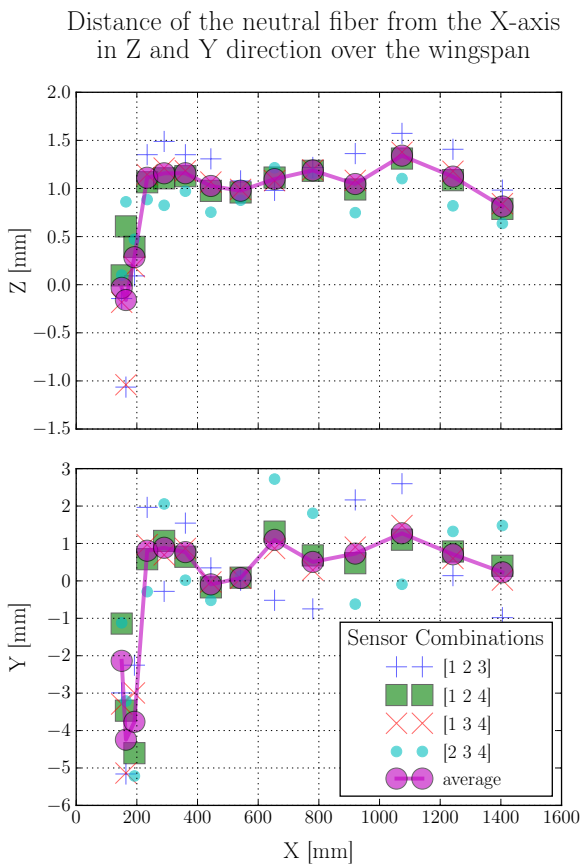

Figure 7: Location of the neutral axis at all 14 cross sections for different sensor combinations.

4.3 Strain Field Calculation

In Section 2.3, a method to separate the measured strain into two directions was presented. In Figure 9, the results of these calculations are shown for all 14 cross sections and five different sensor combinations. The input for the calculations are the measured strain values from 60 sensors (four fibers with each 15 sensors) for a static test case. The Y-axis shows the normalized strain values. Here, normalized means that the values are representing the strain per distance from the neutral axis in Z-direction, respectively in Y-direction. In this test case, a point load was applied at the wing tip in Z-direction. This can be seen with the dimension of the values in Z-direction being about ten times higher than the values in Y-direction. Another way of visualizing the normalized strain values is shown in Fig. 3 exemplary for one cross section.

Visualizing the normalized values for each direction can be useful to identify erroneous sensor data and sensor combinations, or cross sections, where the method and its linear assumption might not be able to accurately calculate the strain for each direction. Due to the reason that the values are normalized, the geometry of the structure has no influence on the values and hence, sudden gradient changes or discontinuous jumps can be traced back to sensor or modeling problems.

Here in this case, the calculated strain values show deviations between the individual sensor combinations for the second, third and fifth cross section (see Fig. 9), for both directions. As a matter of fact, it will be shown in Section 4.4.2 that excluding these cross sections results in a smaller error of the displacement estimation.

4.4 Displacement Calculation

The displacement is calculated using the normalized strain values of the previous chapter. By integrating piecewise over the wingspan, the displacement can be determined for both directions, Z and Y. The displacements at discrete points are fitted to a polynomial regression resulting in a displacement curve. This curve is then compared to results of the photogrammetry measurements. Both curves and the difference between them, the absolute error, are displayed in Fig. 10. The displacement in Z is 118 mm at the wing tip, the absolute error is 4.01 mm. This is a relative displacement error of 3.41%. In Y direction, the displacement is 8.1 mm, the absolute error about 0.71 mm and hence, the relative error is 8.68%. Later, it will be shown that by bypassing certain cross sections for the displacement calculation, the error can be reduced considerably.

	Error Displacement Z		Error Displacement Y	
	Absolute, mm	Relative, %	Absolute, mm	Relative, %
A.) Standard Case - All Sensors used for Calculation of Neutral Axis and Displacement				
1 2 3 4	4.01	-3.41	0.71	8.68
B.) Sensor Combinations used for Displacement Calculation (averaged neutral axis used)				
1 2	4.19	-3.56	0.67	8.18
1 3	11.72	-9.98	-2.83	-34.58
1 4	4.39	-3.73	0.51	6.23
2 3	1.97	-1.68	0.89	10.91
2 4	13.12	-11.17	3.23	39.51
3 4	4.98	-4.23	0.64	7.79
1 2 3	3.50	-2.98	0.67	8.18
1 2 4	4.56	-3.88	0.74	9.09
1 3 4	4.74	-4.03	0.54	6.58
2 3 4	3.94	-3.36	0.82	10.05
C.) Individual Sensor Combinations used for Calculation of Displacement and Neutral Axis				
1 2 3	1.58	-1.34	1.01	12.38
1 2 4	4.29	-3.65	0.62	7.63
1 3 4	4.47	-3.80	0.71	8.69
2 3 4	2.06	-1.75	0.79	9.66
D.) Cross Sections skipped for Displacement Calculation				
1	5.10	-4.34	0.63	7.72
2	3.33	-2.83	0.72	8.85
3	4.55	-3.87	0.58	7.12
4	4.36	-3.71	0.57	7.03
1 2 3	12.00	-10.21	-0.51	-6.25
1 2 3 4	18.08	-15.38	-1.56	-19.04
2 3 4	3.69	-3.14	0.05	0.66
2 3 5	3.48	-2.96	0.51	6.19
2 3 4 5	5.21	-4.43	-0.62	-7.61
2 3 4 5 6	6.55	-5.58	-1.25	-15.25

Table 3: Absolute and relative displacement error at the blade tip (x=1620 mm).

4.4.1 Influence of different Sensor Combinations and different Location of Neutral Axis on Displacement

For this paper, the effect of different sensor combinations used to calculate the displacement was examined. The results of this study are shown in Table 3 and Fig. 8. For case B), the averaged neutral axis was taken as the basis for determining the distances from the sensor location to the neutral axis - which influence the strain field calculations and hence the displacement. Compared to standard case A), the relative error at the wing tip does not differ much for each of the sensor combinations where three sensors per cross section were used: The relative error of the displacement at the wing tip varies from -4.03% to -2.98% in Z, respectively from 6.58% to 10.05% in Y direction. This is valid for both directions, Z and Y. The displacement error for the calculation with two sensors, though, shows significant deviations across the different sensor combinations, ranging from -11.17% to -1.68% in Z, respectively from -34.58% to 39.51% in Y direction. Using only two sensors for the displacement calculation might not be accurate enough. This is particularly true for two sensors which are located diagonally to each other (sensors 1 and 3 or sensors 2 and 4). As a consequence, it might be advisable to use at least three sensors per cross section to calculate the displacement in two directions.

Furthermore, a variation of this case was examined, case C.): Taking for each sensor combination of three sensors per cross section the calculated neutral axis location of these three sensors instead of the averaged neutral axis (see Fig. 7). It can be seen that especially the sensor combinations involving two sensors at the trailing edge show smaller errors in Z direction, compared to the calculation where the averaged neutral axis was taken as a basis.

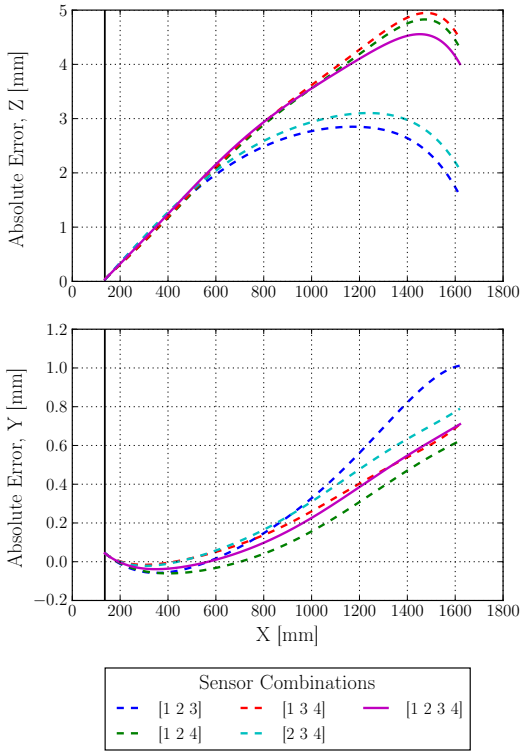

Figure 8: Absolute error of displacement in Z and Y direction for different sensor combinations.

4.4.2 Influence of Skipping Cross Sections

In Section 4.3, the strain field was plotted for each sensor combination. At some cross sections, deviations between the individual sensor combinations are visible. At these cross sections, the assumption of a strain field with a linear gradient might not be thoroughly applicable or other irregularities might be the cause. Therefore, individual cross sections (numbered consecutively with "1" being the cross section at the blade root and "14" being the cross section closest to the wing tip) are skipped at the displacement calculation and the effect on the displacement error is examined. Some of the results are shown in Table 3, case D.). The results were gathered by using all four sensors per cross section. While skipping single cross sections does not have a considerable effect on displacement error, some combinations do reduce the error. For example, skipping cross sections 2/3/4 or 2/3/5 reduces the displacement error in both directions, Z and Y. These excluded cross sections were already identified as possibly problematic in Section 4.3. Other combinations which involve skipping the first four and five cross sections, had negative effects on the displacement error. An explanation for this might be that the first four cross sections are located near the blade root where the highest curvature of the rotor blade is to be expected in this static case. The strain information which can be gathered at these cross sections is important to resolve the curvature of the wing or rotor blade correctly. In general, it might improve the displacement calculations if cross sections are skipped that show deviations among sensor combinations at the strain field calculation.

4.5 Main Sources for Errors and Possible Solutions

While it could be shown above that the method could be successfully applied to a complex rotor blade, calculating the displacement in two directions, the method is subject to various factors which could influence the quality of the results. In the following, the most influential factors are described:

- **Coordinates of the sensors**: When the sensors were bonded to the surface, the coordinates of the sensors in X- and Y-direction were measured by hand. In Z-direction, the thickness of the rotor blade, the coordinates could be extracted from the CAD model. Measurement errors at this point influence the quality of the neutral axis calculation. The calculated location of the neutral axis is shifted to the Y- and/or Z-direction and hence, the displacement calculation is also affected. Comparing the results for different sensor combinations of the neutral axis calculation in order to detect outliers could be a solution to identify sensors with inaccurate coordinates. An example is shown in Section 4.2.
- **Boundary condition (initial angle)**: For the first section of the rotor blade, a boundary condition has to be set for $i = 0$. While it can be assumed safely, that the deflection at that point is $y = 0$ mm, the initial angle might be more difficult to predict. It has been chosen for this paper as $\tan = 0$, but some of the results show evidence, that the angle might not be $0°$. For example, the absolute error in Z-direction in Fig. 8 is linearly increasing from the fixed end to one fourth of the rotor blade radius. This might be caused by the clamp which is not as stiff as expected and bends to a certain degree in reality. Indeed, the angle at the grip could be determined as $-4.5°$ by analyzing the photogrammetry measurements. Using this value as the initial angle results in a lower displacement error. At the moment, there is no solution to this problem.
- **Sensor placement**: The location of the cross sections where strain sensors are applied, is critical in regards to capturing the displacement and the shape of the rotor blade correctly. Ideally, the sensors should be located at cross sections where the first and second derivative of the displacement are zero ($y' = 0$ and $y'' = 0$). While this might be simpler if only the shape of the first eigenmode shall

be determined, it requires an in-depth knowledge of the behavior of the rotor blade, if also higher mode shapes shall be calculated. Missing or not capturing correctly the curvature at a cross section at radius r/R has negative effects on the quality of the results over the whole rest of the length of the rotor blade $1 - r/R$, from that particular cross section up to the tip.

5 CONCLUSION AND OUTLOOK

In this paper, a method was presented to calculate the displacement of a structure in two dimensions from measured strain data at discrete points using FBG sensors. It provides a way to calculate a two-dimensional linear strain field and the resulting displacement without knowledge of the neutral axis. This could be used in the future as an important input for a Health and Usage Monitoring System or for monitoring the wing tip clearance of a coaxial rotorcraft. It has been shown, that the method provides an accurate estimation of the displacement, for both directions. The method was successfully examined at a test bench on a rotor blade with a complex geometry and material build-up. One of the main advantages of the method is the comparability of the neutral axis and strain field calculations by normalizing the strain at each cross section. Thereby, erroneous sensors can be identified more easily. Furthermore, it was shown how, and at which stages of the method, a redundancy concept could be established using distinct sensor combinations and how many different sensors are required.
In a further step, the method will be compared to the modal analysis approach. Additionally, Monte-Carlo simulations are planned to be performed in order to be able to estimate the effect from variations of the boundary conditions, sensor noise and sensor errors on the quality of the neutral axis and displacement calculations. Moreover, dynamic tests will be conducted to examine the ability to capture higher order mode shapes.

ACKNOWLEDGMENTS

The authors would like to thank Julia Blaut and Mark Braun for their commitment to the measurement campaign.

REFERENCES

[1] T.E. Noll et al. “Investigation of the Helios Prototype Aircraft Mishap, Volume I Mishap Report”. In: *NASA, Washington, D.C.* (2004).

[2] European Aviation Safety Agency. “Notice of Proposed Amendment No 2010-12 - Vibration Health Monitoring”. In: (2010).

[3] M. Hajek, S. Manner, and S. Suesse. “Blade Root Integrated Optical Fiber Bragg Grating Sensors – A Highly Redundant Data Source For Future HUMS”. In: *AHS 71st Annual Forum* (2015).

[4] C. Pak. “Wing Shape Sensing from Measured Strain”. In: *AIAA Journal* (2016). DOI: 10.2514/1.J053986.

[5] W.L. Ko, W.L. Richards, and V.T. Tran. “Displacement Theories for In-Flight Deformed Shape Predictions of Aerospace Structures”. In: *NASA TP-2007-214612* (2007).

[6] L.-H. Kang, D.-K. Kim, and J.-J. Han. “Estimation of Dynamic Structural Displacements Using Fiber Bragg Grating Strain Sensors”. In: *Journal of Sound and Vibration, Vol. 305, No. 3* (2007), pp. 534–542.

[7] S. Rapp, L.-H. Kang, U.C. Mueller, and H. Baier. “Dynamic Shape Estimation by Modal Approach Using Fiber Bragg Grating Strain Sensors”. In: *Proceedings of SPIE, Vol. 6529* (2007), 65293E–65304E. DOI: 10.1117/12.715634.

[8] Seung B. Kim, Derek Geiger, Patrick O. Bowles, Claude G. Matalanis, and Brian E. Wake. “Tip Displacement Estimation Using Fiber Optic Sensors for X2 Technology Rotor Blades”. In: *AHS 72nd Annual Forum* (2016).

[9] William L. Ko and Van Tran Fleischer. “Further Development of Ko Displacement Theory for Deformed Shape Predictions of Nonuniform Aerospace Structures”. In: *NASA/TP-2009-214643* (2009).

[10] Christine V. Jutte et al. “Deformed Shape Caluclation of a Full-Scale Wing Using Fiber Optic Strain Data from a Ground Loads Test”. In: *NASA/TP-2011-215975* (2011).

[11] T. Pflumm, A. Barth, K. Kondak, and M. Hajek. “Auslegung und Konstruktion eines Hauptrotorblattes für ein in extremen Flughöhen operierendes Drehflügel-UAV”. In: *DLRK Kongress, Rostock* (2015).

COPYRIGHT STATEMENT

The authors confirm that they, and/or their company or organization, hold copyright on all of the original material included in this paper. The authors also confirm that they have obtained permission, from the copyright holder of any third party material included in this paper, to publish it as part of their paper. The authors confirm that they give permission, or have obtained permission from the copyright holder of this paper, for the publication and distribution of this paper as part of the ERF proceedings or as individual offprints from the proceedings and for inclusion in a freely accessible web-based repository.

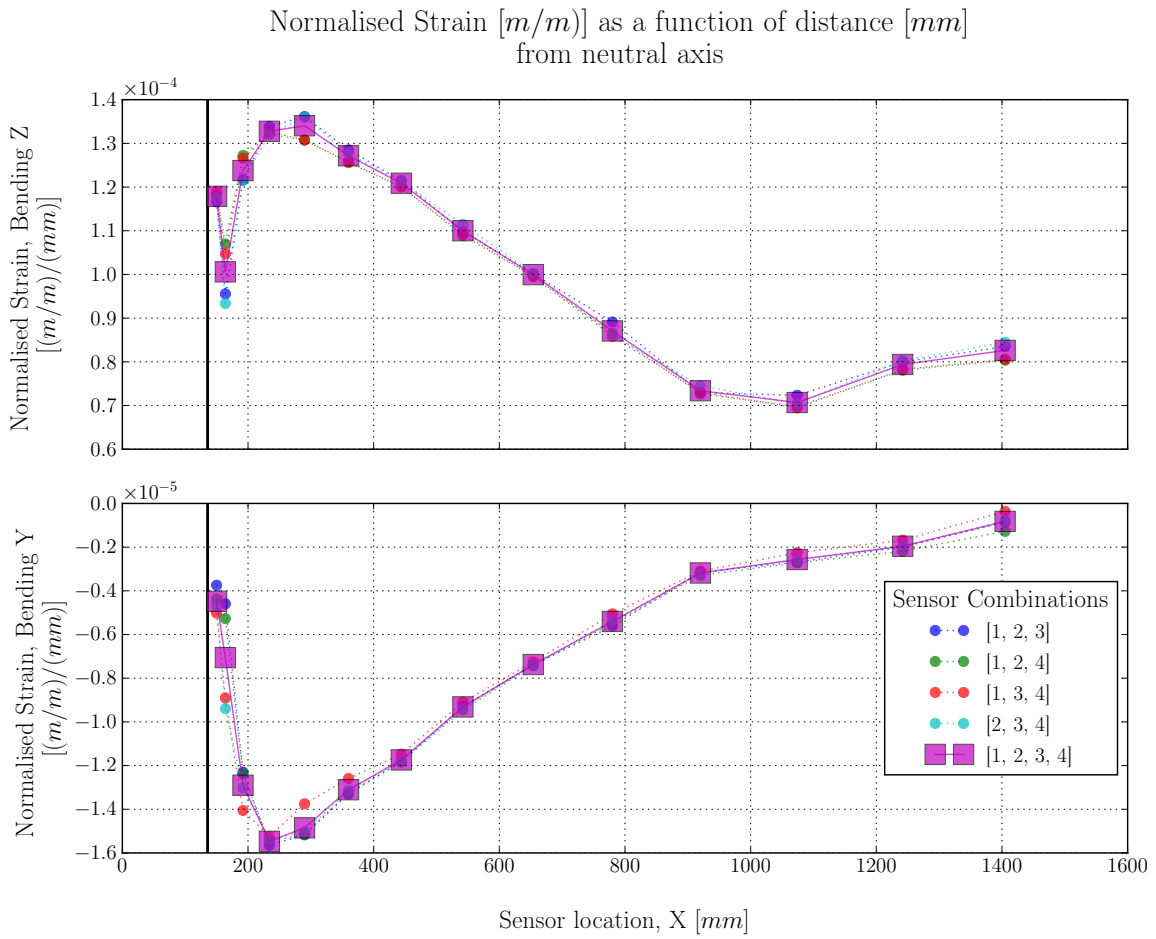

Figure 9: Normalized strain in Z and Y direction for each of the 14 cross sections.

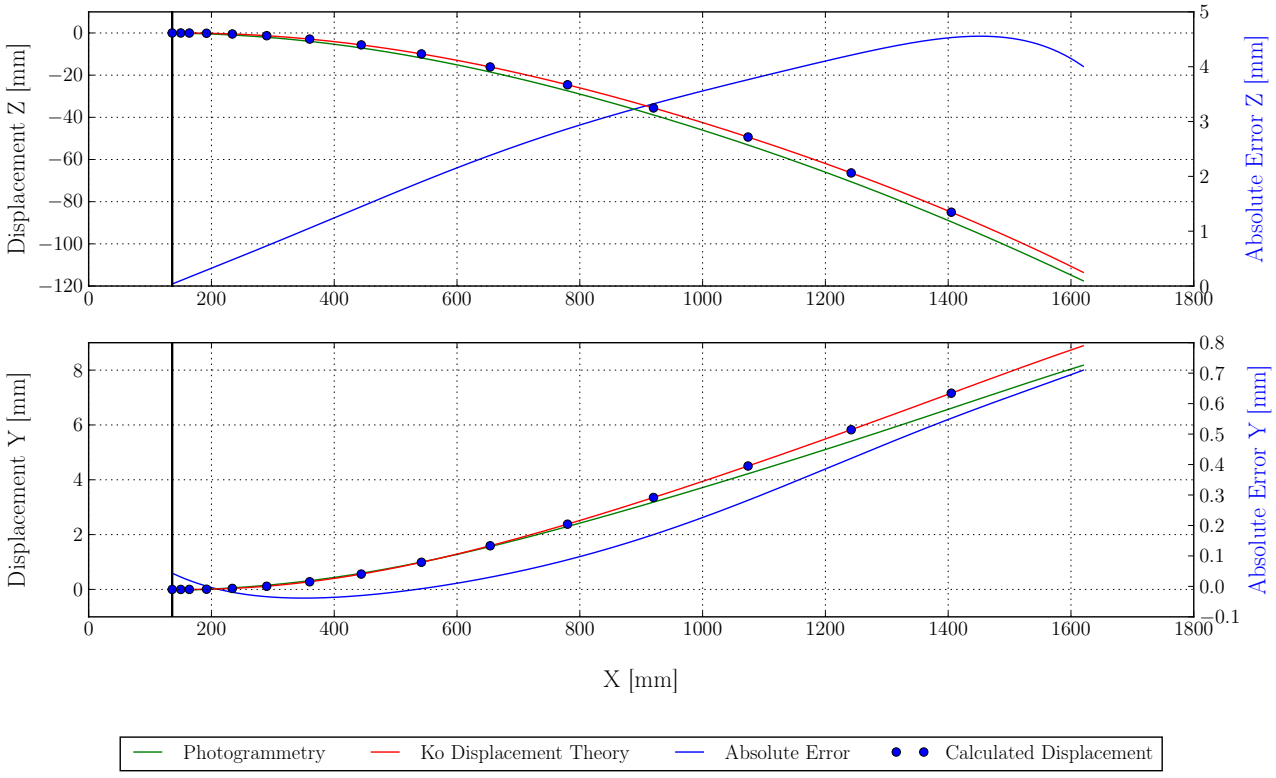

Figure 10: Displacement in Z and Y direction over the wingspan. Comparison between the calculated displacement and the photogrammetry measurements. The absolute error is the difference between both curves.